

**Figure 2** Effective transmission loss of laser fabricated two-port SAW device with free surface (a), 1D (b), and 2D (c) PC structures

where  $K^2$  is the electromechanical coupling constant of the substrate. The mass loading effect on the SAW velocity for a given thickness of aluminium film can be neglected. By substituting values  $V_f = 3488$  m/s and  $K^2 = 4.6\%$  taken from literature [5] into Eqs. (1)–(3) one obtains  $f_B^{(1D)} = 68.25$  MHz, which is in good agreement with the measured value.

With the 2D structure, a considerably stronger and wider drop was observed in the transmission characteristics. The average increase in transmission loss is about 25 dB in the band from 68.25 MHz up to 68.95 MHz. As seen, this band has a lower boundary coinciding with the frequency of 1D peak, and its width is about 0.7 MHz. In the 2D case, the SAW velocity is averaged using the fractions of metallized and free areas as weighting functions [3]:

$$V_{avg}^{(2D)} = \left(\frac{2r}{a}\right)^2 V_m + \left(1 - \left(\frac{2r}{a}\right)^2\right) V_f \quad (4)$$

Calculation with the same parameters as above yields the slightly higher resonance frequency of 68.34 MHz. It is, however, somewhat lower than the experimentally measured mid-band frequency value 68.6 MHz. A more rigorous analysis required to relate the stop-band width to the structure parameters is beyond the scope of this Letter.

## 2. CONCLUSIONS

One-dimensional and two-dimensional SAW PC structures were fabricated on the YZ-LiNbO<sub>3</sub> crystal surface using femtosecond laser micromachining of aluminum thin film. The 1D-structure exhibited peak in the transmission loss at the frequency well described by the Bragg reflection model. The strong enhancement by 25 dB in the 0.7 MHz band of the transmission loss was observed in the 2D-structure. The measured frequency characteristics of the SAW transmission in the structures are in good agreement with theoretical estimations based on the SAW velocity averaged over free and metallized surface of the piezoelectric substrate. The laser technology employed with a maximum resolution of 0.5 μm is shown to be very attractive for fabrication of phononic filters and other complex SAW devices. This technology offers an important advantage of versatile, flexible and multiplex fabrication of sophisticated SAW structures without photolithographical process.

## ACKNOWLEDGMENTS

This work was supported in part by the Research Council of Lithuania under project MIP-125/2010.

## REFERENCES

1. S. Benchabane, A. Khelif, J.-Y. Rauch, L. Robert, and V. Laude, Evidence for complete surface wave band gap in a piezoelectric phononic crystal, *Phys Rev* 30 (2006), 065601-1-4.
2. R. Lucklum and J. Li, Phononic crystals for liquid sensor applications, *Meas Sci Technol* 20 (2009), 124014-1-13.
3. R. H. Olsson, III and I. El-Kady, Microfabricated phononic crystal devices and applications, *Meas Sci Technol* 20 (2009), 012002-1-13.
4. T. Gertus, P. Každailis, R. Rimeika, D. Ciplys, and V. Smilgevičius, Surface acoustic wave transducers fabricated by femtosecond laser ablation, *Electron Lett* 46 (2010), 1175–1176.
5. C.K. Campbell, *Surface acoustic wave devices for mobile and wireless communications*, Academic Press, Orlando, FL, 1998.

© 2012 Wiley Periodicals, Inc.

## PHOTONIC ASYNCHRONOUS DELTA-SIGMA MODULATOR SYSTEM FOR ANALOG-TO-DIGITAL CONVERSION

Azad Siahmakoun,<sup>1</sup> Pablo Constanzo-Caso,<sup>1,2</sup> and Erin Reeves<sup>1</sup>

<sup>1</sup>Department of Physics and Optical Engineering, Rose-Hulman Institute of Technology, 5500 Wabash Avenue, Terre Haute, IN 47803; Corresponding author: siahmako@rose-hulman.edu

<sup>2</sup>Centro de Investigaciones Ópticas (CONICET La Plata—CIC-PBA) and Facultad de Ingeniería Universidad Nacional de La Plata, Camino Centenario y 506, La Plata, BA 1900, Argentina

Received 14 July 2011

**ABSTRACT:** A novel photonic asynchronous delta-sigma modulator (ADSM) has been investigated and demonstrated for the first time in this article. An inverted bistable quantizer is required due to use of a positive feedback in this noninterferometric optical implementation. The principles of the proposed optical first-order and second-order ADSM are modeled and analyzed. Two main components of the novel optical ADSM; the leaky integrator and the inverted bistable quantizer have been mathematically analyzed, simulated, and characterized. Finally, a prototype fiber-optic ADSM is constructed. The prototype operates at MHz frequencies producing four effective-number-of-bits resolution. The reported fiber-optic ADSM is a very promising for future integration of this system on a photonic chip thus increasing the operation frequency range up to tens of GHz. © 2012 Wiley Periodicals, Inc. *Microwave Opt Technol Lett* 54:1287–1292, 2012; View this article online at [wileyonlinelibrary.com](http://wileyonlinelibrary.com). DOI 10.1002/mop.26760

**Key words:** analog-to-digital conversion; delta-sigma modulation; semiconductor optical amplifier; cross gain modulation

## 1. INTRODUCTION

Achieving high-speed, high-resolution analog-to-digital (A/D) conversion is a difficult technological problem. This has largely prohibited the realization of high-speed, high-throughput systems [1]. With fundamental limitations in electronics, greater attention has been turned to using photonic techniques to significantly improve the performance of A/D converters (ADCs) [2, 3]. Benefits of performing A/D conversion in the optical domain include high speed, high information capacity, low timing jitter, and immunity to electromagnetic interference.

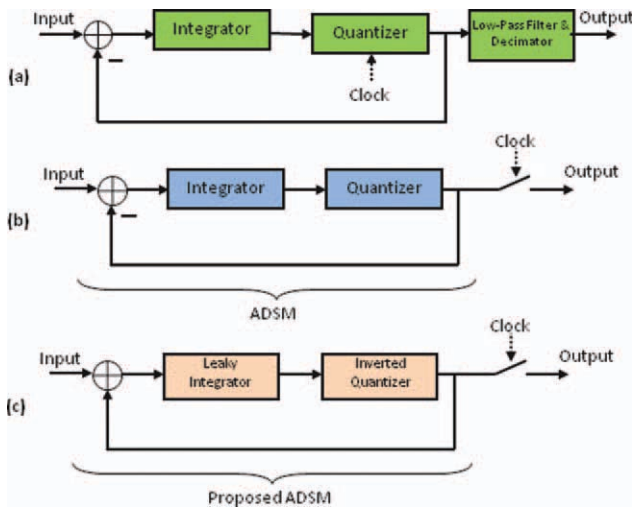


**Figure 1** A/D converters based on (a) DSM, (b) ADSM, and (c) all-positive signals and feedback, ADSM. [Color figure can be viewed in the online issue, which is available at [wileyonlinelibrary.com](http://wileyonlinelibrary.com)]

A delta-sigma-based converter is an oversampled converter, meaning the sampling rate  $f_s$  is much greater than the Nyquist sampling rate  $f_{NY}$  ( $f_{NY} = 2f_B$ , where  $f_B$  is the input signal bandwidth), typically by factors of 8–512 [1]. Delta-sigma modulation (DSM) combined with digital preprocessing/postprocessing is an attractive technique for the conversion of an analog signal into a digitized binary output signal [4]. This kind of converter trades sampling speed for improved amplitude resolution using oversampling, a feedback architecture, linear filtering techniques, and a comparator of modest quality. DSM achieves high-resolution digitalization of narrowband signals through quantization-noise shaping. A first-order, noninterferometric, optical DSM with sampling rate of 1 kHz was demonstrated by Shoop and Goodman [5]. The system uses free-space optics and self-electro-optic effect devices to perform the subtraction and quantization operations. A detailed performance analysis of this converter was developed by Clare et al. [6] resulting with a peak signal-to-quantum-noise ratio of 54 dB and oversampling ratio of 100. A different approach based on a coherent system was proposed by Pace et al. [7] where both the feedback and the quantization are performed in the electrical domain, whereas the subtraction is carried out in the optical domain via a Mach-Zehnder modulator. Subsampling A/D conversion using high-speed, low-jitter photonic sampling and an electronic DSM was demonstrated in Ref. 8. Figure 1(a) shows the basic components of the first-order DSM. The input signal at the left is launched to the system, summed with the negative feedback signal of the previous bit time, integrated, quantized, and then processed by a digital filter.

A slightly different architecture [9], the asynchronous delta-sigma modulator (ADSM), is shown in Figure 1(b). The feedback loop is completely analog, because the sampler is set outside the loop. Neither the clock signal nor digital filtering is required. ADSM turns the amplitude axis over the time axis by producing a binary-amplitude, continuous-time, output signal from an analog input signal. Therefore, to obtain A/D conversion, it is necessary to quantize the time rather than the amplitude as shown in the right side of the figure. This method for A/D conversion does not present the noise shaping property that is one of the advantages of the conventional DSM; however, the ADSM is more robust and easier to design than a high-

frequency DSM, because high-frequency components are not inserted into the loop [10].

In this article, we present a novel photonic ADSM as shown in Figure 1(c). The system is based on a modified architecture of that proposed and theoretically analyzed by Sayeh and Siahmakoun [11]. To the best of our knowledge, this work is the first photonic ADSM demonstrated in the literature. There are two main differences in comparison to the electrical implementation: (i) the proposed device is a noninterferometric optical system, meaning that every signal in the loop is processed as an intensity signal and (ii) an intensity addition is performed between the input and positive-corrective feedback signals since subtraction is a difficult operation to carry out in the optical domain [5, 7].

In this article, we describe our recent progress in photonic ADC. Section 2 presents a background of ADSMs by considering positive feedback and all-positive intensity signals. Section 3 introduces the simulations and practical implementation for the leaky integrator device, and Section 4 shows the experimental results and measured figures of merit of the system. Finally, we conclude the article in Section 5.

## 2. BACKGROUND AND BASIC THEORY

The ADSM is a straightforward conversion processor due to the fact that it does not require any clocking signal and the demodulation step consists of a simple low-pass filtering. The modulator is a closed-loop system, which is built with a linear filter  $H(s)$ , and a nonlinear element is as shown in Figure 2. This ADSM can be considered as a pulse-width modulation system where the duty-cycle,  $D$ , as well as the instantaneous frequency of the modulated output,  $\omega$ , depend on the amplitude of the input signal in the following manner [9]:

$$D(t) = \frac{x(t) + 1}{2} \quad \text{and} \quad \frac{\omega(t)}{\omega_c} = 1 - x^2(t) \quad (1)$$

where  $x(t)$  is the normalized input signal ( $|x(t)| < 1$ ),  $\omega_c$  is the center frequency, and  $D(t) = \alpha(t)/T(t)$  is the instantaneous duty-cycle with  $T(t) = 2\pi/\omega(t)$ .

Because we are interested in a positive feedback-based modulator operating with all positive intensity signals, the nonlinear hysteretic quantizer has to be nonsymmetric, producing a shift in both the input (horizontal) and the output (vertical) axes (see Fig. 2). Therefore, we can rewrite Eq. (1) in a generalized form as:

$$D(t) = -\frac{x(t) - 2}{2} \quad \text{and} \quad \frac{\omega(t)}{\omega_c} = 1 - (x(t) - 1)^2, \quad (2)$$

where the negative slope in the first equation indicates that the duty-cycle increases, as the amplitude decreases and vice versa. As every signal is positive the amplitude of the normalized input satisfies  $0 < x < 2$ .

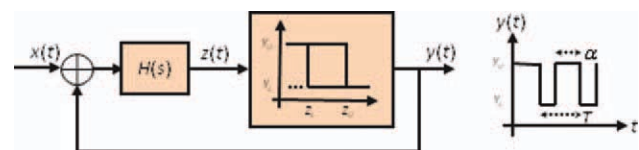


**Figure 2** Block diagram of ADSM and the waveform at the output. [Color figure can be viewed in the online issue, which is available at [wileyonlinelibrary.com](http://wileyonlinelibrary.com)]

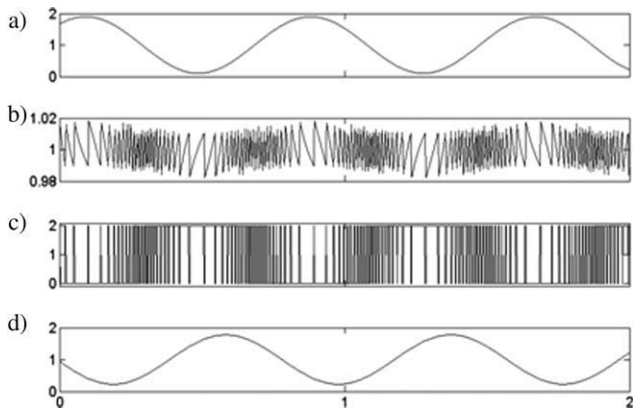


**Figure 3** First-order ADSM simulation results: (a) analog input, (b) integrator output, (c) modulated signal, and (d) recovered signal

The linear filter is a leaky integrator, which has a transfer function given by  $H(\omega) = G/(s + \omega_p)$ , where  $s = i\omega$ ,  $i = (-1)^{1/2}$  is the imaginary unit, and  $G$  is the gain at the pole angular frequency  $\omega_p$ .

The center frequency  $\omega_c$  is defined as the value of the instantaneous frequency, when the input signal has the mean value of the input amplitude ( $x = 1$  for this case). It is the oscillation frequency of the square-wave for a free-running modulator and the highest pulse rate for a forced-oscillation (i.e., for a nonzero input). This frequency depends on the transfer characteristic of the loop filter and the hysteretic quantizer properties as follows:  $\omega_c = (\Delta Y/\Delta Z)/(\pi G/2)$ , where  $\Delta Z = Z_U - Z_L$  and  $\Delta Y = Y_U - Y_L$  are the quantizer input and output ranges, respectively, as depicted in Figure 2.

Notice that both the duty-cycle and the instantaneous frequency are time-dependent and that the amplitude axis can completely be turned over to the time axis without loss of information. It can be viewed as a DSM with infinite sampling frequency. The linearity of the ADSM depends on both the center frequency  $\omega_c$  and the full scale input signal that can be applied to the ADSM. For higher center frequencies, the first harmonic band centered around  $\omega_c$  is far enough away from the baseband frequency components (where the information is contained), so aliasing is not a concern for the band of interest. For larger amplitude input signals (high modulation depth), the modulator is overloaded, and the modulated output signal will be distorted. On the other hand, smaller inputs generate modulated outputs close to the center frequency with a duty-cycle around 50%.

### 3. NUMERICAL SIMULATIONS

Several important differences can be observed between the conventional and the proposed ADSM: the negative feedback is now positive, the integrator is now a leaky integrator, the bistable quantizer is now an inverted bistable quantizer, and the input signals are now positive. The difference between an integrator and a leaky integrator is that the leaky integrator simultaneously integrates the input and gradually leaks a small part of the accumulated energy.

To realize the photonic ADSM, the output of the bistable hysteretic quantizer is required to be inverted, that is, a high output for low input and vice versa. This configuration can be seen as a pseudonegative feedback, because a low feedback signal is added to a high input signal, and a high feedback signal is applied to a low input signal. The hysteresis curve of the

inverted bistable quantizer is shown in the corresponding block in Figure 2. The values  $Z_L$  and  $Z_U$  are the respective switching ON and OFF points, and the output of the quantizer is determined by the upper and lower levels,  $Y_U$  and  $Y_L$ , respectively.

The first-order ADSM is simulated using the Simulink software. Without loss of generality, every amplitude value is normalized to 1 V to avoid writing absolute magnitudes. The dynamic range of the modulator is 2. The sinusoidal input signal launched into the loop has a peak-to-peak and bias voltage of 1.8 and 1 (i.e., the modulation depth is 90%), respectively, and a frequency of 1.25 MHz. The leaky integrator presents a pole frequency of  $10/2\pi$  MHz and a gain of 5. The inverted bistable quantizer ON and OFF switching points were set to 1.01 and 0.99, respectively, and the output signal upper and lower levels were set to 2 and 0, respectively. Finally, the demodulator is implemented with a second-order low-pass Butterworth filter with a second-order pole at the frequency of  $20/2\pi$  MHz. Figures 3(a)–(d) show the simulated signals at different points of the ADSM: (a) analog input, (b) integrator output, (c) modulated signal, and (d) demodulated signal. A result of using the inverted bistable quantizer is that the output binary is also inverted. This effect can be easily seen comparing Figures 3(a) and (d). Here, the recovered signal is shown to be shifted from the input sinusoid by  $\pi$ . The demodulated signal indicates that the binary output contains all the input signal information, confirming proper operation of the modulator.

Before the experiment and results are presented, the photonic leaky integrator will be briefly discussed. A complete analysis and mathematical theory of the photonic integrator is discussed in Ref. 12. Figure 4 shows the basic setup of the photonic leaky integrator. The integrator loop consists of a semiconductor optical amplifier (SOA) gain element, a hybrid band-pass filter, and isolator component to select the loop wavelength and ensure unidirectional propagation, and two couplers, optical coupler (OC)<sub>1</sub> and OC<sub>2</sub>. OC<sub>1</sub> is used to combine the input and circulating loop signals and launch them into the integrator loop, and OC<sub>2</sub> extracts part of the circulating signal as the output signal.

To avoid interference effects between the input and circulating signals, wavelength conversion is performed from input wavelength  $\lambda_1$  to a different wavelength  $\lambda_2$  that is defined by the band pass filter. The wavelength conversion is accomplished by the cross-gain modulation (XGM) phenomenon in the SOA. Basically, the input wavelength  $\lambda_1$  is used to modify the SOA's gain: a higher gain is achieved for low input powers, otherwise a lower gain is realized. The circulating signal at  $\lambda_2$  decreases with high input signals at  $\lambda_1$  and increases with low input signals at  $\lambda_1$ ; that is, the  $\lambda_2$  signal experiences the SOA gain. An effect of using wavelength conversion to avoid feedback

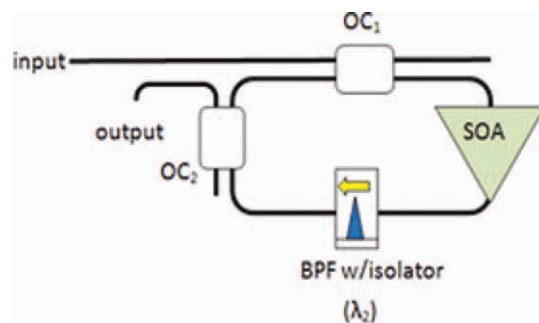


**Figure 4** Photonic leaky integrator setup. [Color figure can be viewed in the online issue, which is available at [wileyonlinelibrary.com](http://wileyonlinelibrary.com)]

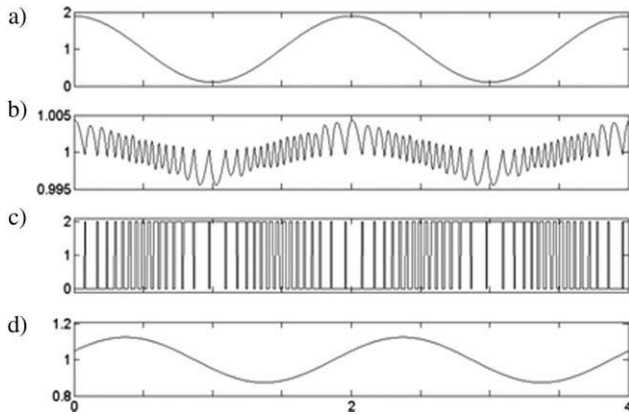


**Figure 5** Second-order ADSM simulation results: (a) analog input, (b) integrator output, (c) modulated signal, and (d) recovered signal

interference is an inverted output: the output is low for high inputs and otherwise.

To realize the ADSM system presented in Figure 2, a method to correct the inverted output of the leaky integrator is required. Signal inversion can be achieved by cascading two inverted leaky integrators. As the inverted output of the first integrator will be inverted by the second integrator again, the output of the second integrator will correspond to the initial input signal launched into the system. However, the alternative approach is to use a noninverted quantizer and have a first-order ADSM architecture [13].

Therefore, a novel device including two inverted leaky integrators is simulated to confirm its feasibility. The photonic inverted leaky integrator can be modeled by a transfer function similar to the one presented in Section 2 for a noninverted leaky integrator. The exceptions include a negative gain for signal inversion and a DC offset to ensure all-positive signal values. The parameters are set as  $G = -5$ ,  $\omega_p = 10/2\pi$  MHz, and the DC value  $h_{DC} = 1$ . The inverted bistable quantizer ON and OFF switching points are set to 1.001 and 0.999, respectively. The output signal upper and lower levels are set to  $Y_U = 2$  and  $Y_L = 0$ , respectively, and the input sinusoid signal has a bias value of 1 and a peak-to-peak amplitude of 1.8. The dynamic range of the ADSM is 2, and thus the corresponding modulation depth is 90%. A second-order low-pass Butterworth filter was used to demodulate the output binary signal, having a cutoff frequency of  $20/2\pi$  MHz. Figures 5(a)–(d) show the input, second-order integrator output, modulated and recovered signals, respectively. Again, the output binary and demodulated signals are inverted due to the inverted bistable quantizer. Also notice that the second-order integrator output is smoother than the corresponding output of the first-order integrator. This, in turn, results in an improved signal-to-noise ratio (SNR) of the modulated signal for the second-order ADSM.

The simulation of the proposed second-order ADSM confirms that this system produces the correct modulated output. It could be used to perform an A/D conversion, if a sampling device is placed at the output of the system as shown in Figure 1(c). The novel second-order optical ADSM is constructed in our laboratory, and the experiment and results are discussed in the next section.

#### 4. EXPERIMENTS

The photonic ADSM setup is illustrated in Figure 6. An electric RF signal of amplitude 2 Vpp and offset  $-1$  V is used to modu-

late a Fujitsu FLD5F10NP continuous wave (CW) laser operating at  $\lambda_1 = 1553.16$  nm by electro-absorption modulation (EAM). The CW laser output is coupled into the system with a 3 dB coupler and coupled into a leaky integrator via OC<sub>1</sub>. The integrator uses the XGM effect of a Kamelian OPA-20-N-C-FP SOA and a Lightel hybrid bandpass filter and isolator of center wavelength  $\lambda_2 = 1551.48$  nm to convert the signal wavelength to  $\lambda_2$ . The output of the first leaky integrator is split by OC<sub>2</sub> where a portion of the signal is used as feedback to complete the 1-m long integrator loop. The wavelength conversion causes the integrator output to be inverted, and thus a second leaky integrator is introduced to correct this signal inversion by inverting the signal again. The second integrator operates in a similar fashion as the first integrator and converts the optical signal from  $\lambda_2$  back to  $\lambda_1$ . It is comprised of a second Kamelian OPA-20-N-C-FP SOA and a Lightel hybrid bandpass filter of center wavelength  $\lambda_1$ .

The output is detected by a photodetector, and the corresponding electrical signal is sent through a quantizing circuit based on the Texas Instruments TLV 3502 comparator chip. The comparator output is used to modulate a second Fujitsu FLD5F10NP CW laser by EAM to provide feedback to the system. A 90/10 coupler is used to split the feedback signal where 90% is sent back through the system as feedback and 10% is detected and observed on an oscilloscope as the delta-sigma modulated signal.

To fulfill the power balance requirements, the input and feedback laser powers and SOA gains are adjusted by controlling their respective driving currents. The currents are set to 70 and 50 mA for the input and feedback lasers, respectively. The SOA

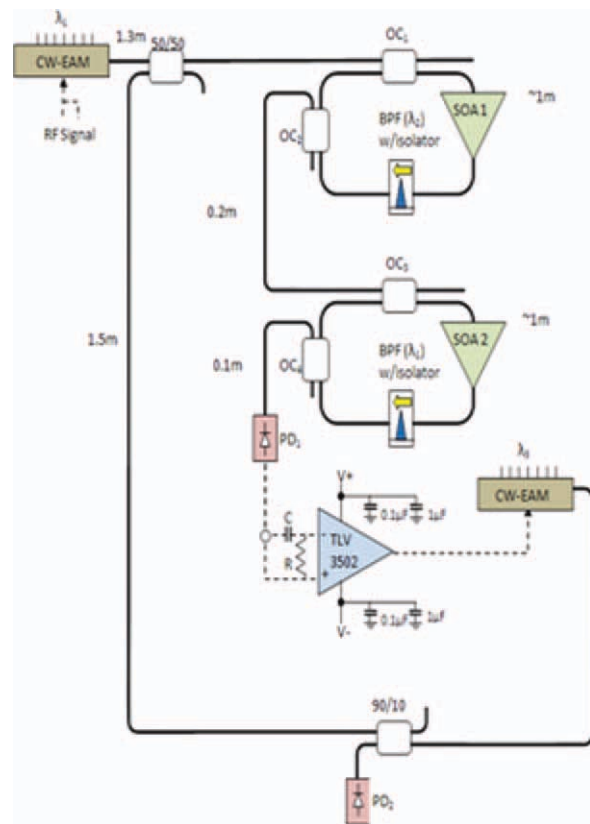


**Figure 6** Experimental setup for photonic ADSM (EAM: electro-absorption modulator, BPF: band pass filter, PD: photodetector). [Color figure can be viewed in the online issue, which is available at [wileyonlinelibrary.com](http://wileyonlinelibrary.com)]

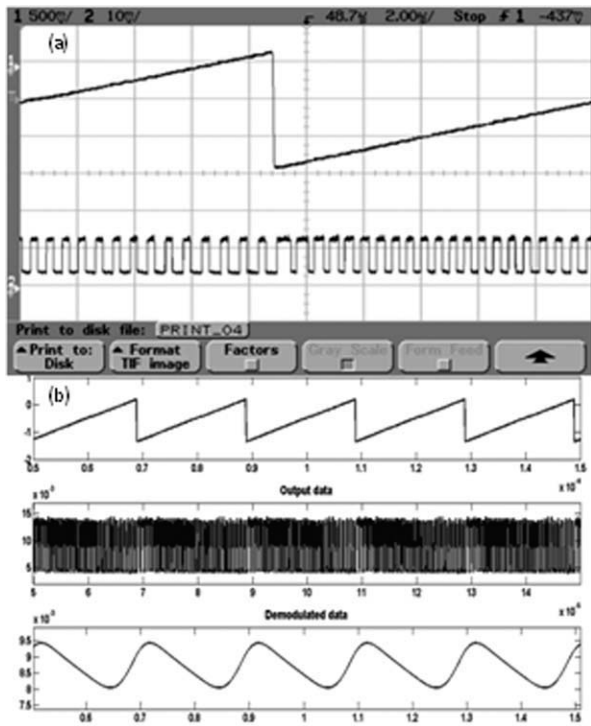


**Figure 7** (a) Second-order ADSM response for a 50 kHz saw tooth input signal (top) and binary output (bottom), and (b) the same signals acquired in a PC (top and middle traces) and the corresponding demodulated output (bottom)

current in the integrator one is set to 70 mA, and the SOA current of the second integrator is 90 mA.

To perform measurements of the ADSM, a saw-tooth waveform is used to show the linearity of the modulator, and sinusoidal inputs are used to test the frequency response. Figure 7(a) shows the ADSM saw-tooth input at frequency 50 kHz (top trace) and the corresponding binary output (bottom trace), which are observed using an oscilloscope. Figure 7(b) also shows these same signals, when acquisition is performed using a personal computer (PC). In this case, demodulation is performed using a MATLAB-based program to verify that the binary output describes the inverse of the analog input signal. The corresponding demodulated output is shown in the bottom trace of Figure 7(b) where the signal inversion can be clearly observed. The high-frequency transition, typical in this kind of waveforms, cannot be properly modulated due to the limited bandwidth of the ADSM. For this reason, the demodulated output shows a smoother change at the saw-tooth edges compared to the input. However, the modulator shows a very good response between signal edges.

Next, measurements for higher frequency sinusoidal inputs are presented. Figures 8(a)–(c) show the ADSM inputs (top traces) and binary outputs (bottom traces) at frequencies between 0.5 to 2 MHz. Again, the signal inversion can be observed in the binary output. When the input signal is at a maximum, a majority of the bits are at the low level, and when the input signal is at its minimum, output bits are high. The 2-MHz binary output is imported into the PC and processed with a MATLAB-based code. The acquired signal is filtered using a third-order Butterworth filter with cutoff frequency at 2.1 MHz. The ADSM input, modulated binary output, and demodulated signals are illustrated in Figure 8(d). It can be seen that the recovered signal, although inverted, appropriately describes the

analog input frequency. By comparing traces in Figure 7 to those in Figure 8, it can be observed that the number of output binary pulses decreases as the input signal frequency increases. For the 2 MHz input, the modulator is operating at the limit of its bandwidth, because just a few pulses are observed per period of the input signal.

The photonic ADSM maximum input frequency can be limited by two factors: the first is the time delay introduced by the optical fiber length, specifically the integrator loop and the feedback, and the second is the speed of the quantizing circuit. The time delay introduced by the fiber is given as  $t = (n_{\text{eff}}L)/c$ , where  $n_{\text{eff}}$  is the index of refraction of the fiber,  $L$  is the fiber

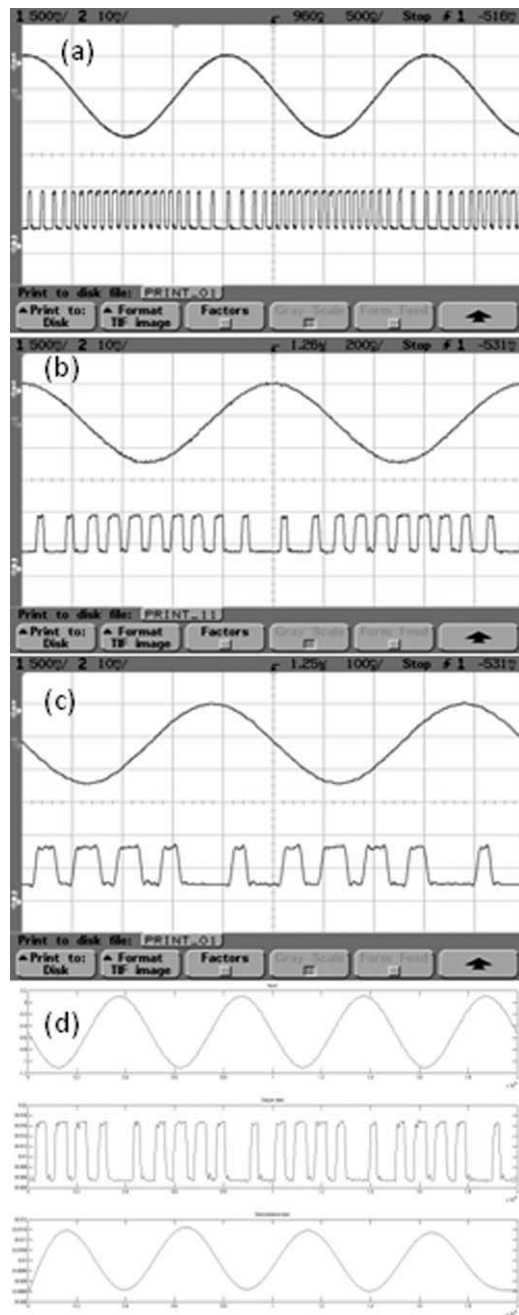


**Figure 8** Second-order ADSM sinusoid input signal (top trace) and corresponding binary output (bottom trace) at (a) 0.5 MHz, (b) 1 MHz, and (c) 2 MHz frequencies. (d) The same 2 MHz input and binary signals (top and middle traces), shown in (c), and the corresponding demodulated output (bottom trace)

length, and  $c$  is the speed of light in vacuum. In our photonic ADC, the loop lengths of the integrators are 1 m each, which leads to a free-spectral range of 200 MHz. If 10–20 round trips per period are desired, then the input frequency must not exceed the 10–20 MHz range. The 1.5 m feedback length introduces a delay of 7.5 ns. This delay has to be much smaller than the input period to effectively provide the ADSM's corrective feedback. Thus, the input frequency should be smaller than 13 MHz. Finally, the current speed limitation we have encountered is due to the quantizing circuitry rather than the length of fiber pigtailed. In order to have a high transition rate, the quantizer must operate at speeds much greater than the input signal. Currently, the quantizing circuit operates well for frequencies up to about 20 MHz. Therefore, to obtain modulated outputs presenting a high density of pulses, the input frequency has to be much smaller than 20 MHz (i.e., maximum 1–2 MHz to allow oversampling of  $20\times$ – $10\times$ ) as is observed in the above-mentioned measurements.

The performance of the ADSM is limited by noise and nonlinearities. Figures of merit such as SNR, the effective-number-of-bits (ENOB), and spur-free dynamic range can be used to characterize the modulator. The ENOB is the resolution of the ADSM without considering the quantization noise, that is, it represents an upper band limitation for the photonic ADC resolution.

The signal-to-noise and distortion ratio (SINAD) is measured over a bandwidth of 1 MHz, and the fast Fourier transform of the acquired signals is used to make the calculations. The measured values are  $\text{SINAD} = 26$  dB, which corresponds to  $\text{ENOB} \cong 4$ . Notice that in these measurements and calculations, the noise sources (shot, thermal, and relative intensity noise) as well as signal distortions are all taken into account.

In conclusions, we have presented our progress toward a photonic ADC based on ADSM architecture. The proposed device, in our knowledge, is the first photonic ADSM demonstrated in the literature. The system includes two leaky integrators and an inverted hysteretic quantizer inside a positive-feedback fiber-optic loop. The system overcomes the limitations set by coherent designs, such as high noise, signal fluctuations, and the difficulty to perform optical subtraction.

The proposed device operates in the MHz range. While the demonstrated system is limited to  $\sim 2$  MHz to achieve a minimum pulse density per cycle, the system has been shown to provide predictable binary output at higher frequencies. The characterized ADSM has a performance of 4 ENOB (or  $\text{SINAD} = 26$  dB) operating at a bandwidth of 1 MHz. This result can be improved by a fine adjustment of the active component parameters (e.g., SOA and laser currents, comparator parameters, etc.), replacing the quantizing circuitry with a high-speed comparator, and reducing the fiber pigtailed of the components. The simulations and experimental implementation suggest that the optical ADSM has the potential to work in the GHz range by photonic integration of the system on a chip to reduce the optical path in the integrator and feedback loops, and using high-speed optical quantizer with switching time better than 100 ps [14].

Finally, to develop the ADSM-based ADC, as shown in Figure 1(c), a photonic sampler is to be connected at the output of the system. Photonic samplers using optical pulse trains from mode-locked lasers have been successfully applied in ADCs [8]. This laser presents ultrashort pulse-width ( $<100$  fs) and ultralow timing jitter ( $<5$  fs) making it possible to develop a high-resolution and high-bandwidth photonic ADC.

## ACKNOWLEDGMENTS

This work was partially supported by Indiana RF Alliance, Poly-phase Microwave, Inc., TSC and NSWC-Crane Division, Crane, IN. Pablo A. Costanzo Caso acknowledges the support of CONICET (PIP 112-200801-01769), Facultad de Ingeniería Universidad Nacional de La Plata (Project I128), and ANPCyT (PICT 0378/08 and 38289/05).

## REFERENCES

1. R.H. Walden, Analog-to-digital converter survey and analysis, *IEEE J Sel Areas Commun* 17 (1999), 539–550.
2. G.C. Valley, Photonic analog-to-digital converters, *Opt Express* 15 (2007), 1955–1981.
3. B.L. Shoop, Photonic analog-to-digital conversion, Springer, New York, 2000.
4. R. Schreier, G.C. Temes, Understanding delta-sigma data converter, Wiley/IEEE Press, New York, 2004.
5. B.L. Shoop and J.W. Goodman, A first-order error diffusion modulator for optical oversampled A/D conversion, *Opt Commun* 97 (1993), 167–172.
6. B.A. Clare, K.A. Corbett, and K.J. Grant, Performance of a photonic oversampled sigma-delta quantizer, *Proc SPIE* 5814 (2005), 248–261.
7. P.E. Pace, S.A. Bewley, and J.P. Powers, Fiber-lattice accumulator design considerations for optical  $\Sigma\Delta$  analog-to-digital converters, *Opt Eng* 39 (2000), 1517–1526.
8. J. Kim, M.J. Park, M.H. Perrott, and F.X. Kärtner, Photonic sub-sampling analog-to-digital conversion of microwave signals at 40-GHz with higher than 7-ENOB resolution, *Opt Express* 16 (2008), 16509–16515.
9. S. Ouzounov, E. Roza, J.A. Hegt, G. van der Weide, and A.H.M. Roermund, Analysis and design of a high-performance asynchronous sigma-delta modulator with binary quantizer, *IEEE J Solid-State Circuits* 41 (2006), 588–596.
10. E. Roza, Poly-phase sigma-delta modulation, *IEEE Trans Circuits Syst II* 44 (1997), 915–923.
11. M.R. Sayeh and A. Siahmakoun, All optical binary delta-sigma modulator, *Proc SPIE* 5970 (2005), 59700P.
12. P.A. Costanzo-Caso, Y. Jin, S. Granieri, and A. Siahmakoun, Optical leaky integrator with inverted and non-inverted accumulation, *Microwave Opt Technol Lett* 53 (2011), 2034–2037.
13. E.M. Reeves, P.A. Costanzo-Caso, and A. Siahmakoun, Asynchronous first-order fiber-optic delta-sigma modulator, *J Opt Eng*, submitted for publication.
14. P.A. Costanzo-Caso, M. Gehl, S. Granieri, and A. Siahmakoun, Optical bistable switching with symmetrically-configured SOAs in reverse bias, *Microwave Opt Technol Lett* 52 (2010), 2753–2759.

© 2012 Wiley Periodicals, Inc.

## A COMPACT UWB SLOT ANTENNA WITH SIGNAL REJECTION IN 5–6 GHz BAND

Akkala Subbarao and S. Raghavan

Department of Electronics and Communication Engineering,  
National Institute of Technology, Tiruchirappalli, Tamilnadu, India;  
Corresponding author: subbarao\_ka@yahoo.com

Received 14 July 2011

**ABSTRACT:** In this article, a novel planar slot antenna is presented with band-notched characteristic for ultra wideband applications. The antenna is fed by coplanar wave guide. A “C” shaped slot etched on the radiating patch to avoid interference from WLAN and HYPERLAN/2 bands. The antenna has measured bandwidth ranging from 3 to 10.6 GHz for  $\text{VSWR} \leq 2$ . The antenna has omni directional radiation pattern in H-plane and bi-directional in E-plane. The group delay of antenna is less than 1 ns except in the notched band. Good agreement is found